



MSU Graduate Theses

Summer 2018


Investigations on Hydrothermally Synthesized Co₃O₄/ Mn_xCo_{3-x}O₄ Core-Shell Nanoparticles

Ning Bian

Missouri State University, Bian0627@live.missouristate.edu

As with any intellectual project, the content and views expressed in this thesis may be considered objectionable by some readers. However, this student-scholar's work has been judged to have academic value by the student's thesis committee members trained in the discipline. The content and views expressed in this thesis are those of the student-scholar and are not endorsed by Missouri State University, its Graduate College, or its employees.

Follow this and additional works at: <https://bearworks.missouristate.edu/theses>

 Part of the [Nanoscience and Nanotechnology Commons](#), and the [Other Materials Science and Engineering Commons](#)

Recommended Citation

Bian, Ning, "Investigations on Hydrothermally Synthesized Co₃O₄/Mn_xCo_{3-x}O₄ Core-Shell Nanoparticles" (2018). *MSU Graduate Theses*. 3311.

<https://bearworks.missouristate.edu/theses/3311>

This article or document was made available through BearWorks, the institutional repository of Missouri State University. The work contained in it may be protected by copyright and require permission of the copyright holder for reuse or redistribution.

For more information, please contact bearworks@missouristate.edu.

**INVESTIGATIONS ON HYDROTHERMALLY SYNTHESIZED $\text{Co}_3\text{O}_4/\text{Mn}_x\text{Co}_{3-x}\text{O}_4$
CORE-SHELL NANOPARTICLES**

A Master's Thesis

Presented to

The Graduate College of

Missouri State University

In Partial Fulfillment

Of the Requirements for the Degree

Master of Science, Materials Science

By

Ning Bian

August 2018

Copyright 2018 by Ning Bian

INVESTIGATIONS ON HYDROTHERMALLY SYNTHESIZED $\text{Co}_3\text{O}_4/\text{Mn}_x\text{Co}_{3-x}\text{O}_4$ CORE-SHELL NANOPARTICLES

Physics, Astronomy and Materials Science

Missouri State University, August 2018

Master of Science

Ning Bian

ABSTRACT

Two different morphologies (pseudo-spherical shaped or PS type and hexagonal nanoplate shaped or NP type) and two different concentrations (0.07 M and 0.1 M) of manganese incorporated $\text{Co}_3\text{O}_4/\text{Mn}_x\text{Co}_{3-x}\text{O}_4$ core-shell nanoparticles (CSNs) were investigated, respectively. The motivation of this work is to investigate the magnetic properties of, and specifically the exchange bias, between different shaped CSNs and between different Mn-doped CSNs. A two-step synthesis method was utilized to obtain the CSNs: a soft chemical approach was used to obtain Co_3O_4 nanoparticles and a hydrothermal nano-phase epitaxy was used to obtain inverted bimagnetic core-shell nanoparticles. XRD results showed that $F\bar{4}3m$ crystal symmetry persists throughout the core region and the shell region for both of PS type and NP type CSNs. TEM-EDX results confirmed that manganese ions were successfully incorporated into the Co_3O_4 spinel structure of the CSNs. TEM and SEM result confirmed that there is no change in shape after the hydrothermal treatment. HRTEM results showed that the core and the shell can be easily distinguished by the interface between the two regions. Magnetic measurements showed that PS type CSNs have a higher coercivity and exchange bias than NP type CSNs at 5K. The XPS results confirmed that Mn ions were incorporated in the 2+ oxidation state in the CSNs.

KEYWORDS: CSNs, Co_3O_4 , $\text{Mn}_x\text{Co}_{3-x}\text{O}_4$, exchange bias, magnetism

This abstract is approved as to form and content

Robert A. Mayanovic, PhD
Chairperson, Advisory Committee
Missouri State University

**INVESTIGATIONS ON HYDROTHERMALLY SYNTHESIZED $\text{Co}_3\text{O}_4/\text{Mn}_x\text{Co}_{3-x}\text{O}_4$
CORE-SHELL NANOPARTICLES**

By

Ning Bian

A Master's Thesis
Submitted to the Graduate College
Of Missouri State University
In Partial Fulfillment of the Requirements
For the Degree of Master of Science, Materials Science

August 2018

Approved:

Robert A. Mayanovic, PhD

Ridwan Sakidja, PhD

Fei Wang, PhD

Julie Masterson, PhD: Dean, Graduate College

In the interest of academic freedom and the principle of free speech, approval of this thesis indicates the format is acceptable and meets the academic criteria for the discipline as determined by the faculty that constitute the thesis committee. The content and views expressed in this thesis are those of the student-scholar and are not endorsed by Missouri State University, its Graduate College, or its employees.

ACKNOWLEDGEMENTS

I would like to give my biggest thanks to Dr. Robert A. Mayanovic, without whose guidance in my research work and in my life, I could not have finished my master's study at MSU. Dr. Mayanovic is insightful and knowledgeable; I learned a lot from him in research and attitude of life. I know what I have learned from him is just a little bit and I wish I could learn more from him in future. I am grateful to Dr. Kartik Ghosh. He is a skillful Professor who helped me a great deal in tutoring me to use instrumentation skillfully. I would be remiss if I did not thank Dr. Ridwan Sakidja: he is versatile not only in computation but also in many other areas. I am also grateful to Dr. David Cornelison: he granted me a great favor during my graduate studies. I am also grateful to Mr. Rithi Patel of Jordan Valley Innovation Center and Dr. Mourad Benamara from University of Arkansas, and thank them for their help with instrumentation and sample characterization. Thanks also to the graduate students and other faculty members of PAMS; I enjoyed my time spent with you. Thank you to the entire department of Physics Astronomy and Materials Science and MSU, BEARS UP!

I dedicate this thesis to my loving parents and my loving wife.

TABLE OF CONTENTS

Chapter 1: Introduction.....	1
Chapter 2: A Study of Different Morphologies of Manganese Incorporated Core-Shell Nanoparticles	7
Abstract.....	7
Introduction.....	8
Experimental.....	9
Characterization	11
Results and Discussion	12
Conclusions	21
References	22
Chapter 3: A Study of Concentration Dependent of Manganese Incorporated Core-Shell Nanoparticles	24
Abstract.....	24
Introduction.....	25
Experimental.....	26
Characterization.....	27
Results and Discussion	28
Conclusions	34
References	35
Chapter 4: Summary	36
References.....	37

LIST OF TABLES

Table 2.1 Experimental parameters of two different morphologies CSNs.....	10
Table 2.2 Chemical composition of two different morphologies CSNs obtained from XPS data.....	21
Table 3.1 Chemical composition of 0.1M CSNs obtained from XPS data.....	32

LIST OF FIGURES

Fig. 1.1 Classic model of exchange bias phenomenon. Magnetization vs. field hysteresis loop is shifted along the field axis at $T < T_N$ [8].....	3
Fig. 1.2 Normal spinel structure of cobalt oxide (Co_3O_4).....	4
Fig. 1.3. The hypothetical structure of $\text{Co}_3\text{O}_4@\text{Mn}_x\text{Co}_{3-x}\text{O}_4$ core-shell nanoparticles. The purple circles are Mn ions incorporated in the tetrahedral sites.	5
Fig. 2.1 (a) A SEM image of the PS type Co_3O_4 nanoparticles; (b) a SEM image of the NP type Co_3O_4 nanoparticles	14
Fig. 2.2 (a) A TEM image of the PS type $\text{Co}_3\text{O}_4@\text{Mn}_x\text{Co}_{3-x}\text{O}_4$ CSNs; (b) Corresponding Size distribution of the PS type $\text{Co}_3\text{O}_4@\text{Mn}_x\text{Co}_{3-x}\text{O}_4$ CSNs	14
Fig. 2.3 (a) A TEM image of the NP type $\text{Co}_3\text{O}_4@\text{Mn}_x\text{Co}_{3-x}\text{O}_4$ CSNs; (b) Corresponding diameter distribution of the NP type $\text{Co}_3\text{O}_4@\text{Mn}_x\text{Co}_{3-x}\text{O}_4$ CSNs; (c) Corresponding thickness distribution of the NP type $\text{Co}_3\text{O}_4@\text{Mn}_x\text{Co}_{3-x}\text{O}_4$ CSNs	14
Fig. 2.4 A high-resolution TEM image of PS type $\text{Co}_3\text{O}_4@\text{Mn}_x\text{Co}_{3-x}\text{O}_4$ CSNs	15
Fig. 2.5 XRD patterns of $\text{Co}_3\text{O}_4@\text{Mn}_x\text{Co}_{3-x}\text{O}_4$ CSNs: (a) PS type $\text{Co}_3\text{O}_4@\text{Mn}_x\text{Co}_{3-x}\text{O}_4$ CSNs; (b) NP type $\text{Co}_3\text{O}_4@\text{Mn}_x\text{Co}_{3-x}\text{O}_4$ CSNs.....	16
Fig. 2.6: (a) FC and ZFC hysteresis loops measured from PS type $\text{Co}_3\text{O}_4@\text{Mn}_x\text{Co}_{3-x}\text{O}_4$ CSNs at 5 K; (b) FC and ZFC hysteresis loops measured from NP type $\text{Co}_3\text{O}_4@\text{Mn}_x\text{Co}_{3-x}\text{O}_4$ CSNs at 5 K; the insets show enlarged views of the M vs H data	18
Fig. 2.7: (a) FC and ZFC magnetization vs. temperature data of PS type $\text{Co}_3\text{O}_4@\text{Mn}_x\text{Co}_{3-x}\text{O}_4$ CSNs; (b) FC and ZFC magnetization vs. temperature data of NP type $\text{Co}_3\text{O}_4@\text{Mn}_x\text{Co}_{3-x}\text{O}_4$ CSNs; the insets show enlarged views of M vs. T data. The FC and ZFC data were measured at an applied field of 300 Oe. The FC hysteresis measurements were made with the samples cooled from 300 K to 5 K at 20,000 Oe	18
Fig. 2.8 Coercivity vs. temperature data of: (a) NP type $\text{Co}_3\text{O}_4@\text{Mn}_x\text{Co}_{3-x}\text{O}_4$ CSNs, (b) PS type $\text{Co}_3\text{O}_4@\text{Mn}_x\text{Co}_{3-x}\text{O}_4$ CSNs.....	19
Fig. 2.9 Exchange Bias vs. temperature data of: (a) NP type $\text{Co}_3\text{O}_4@\text{Mn}_x\text{Co}_{3-x}\text{O}_4$ CSNs, (b) A PS type $\text{Co}_3\text{O}_4@\text{Mn}_x\text{Co}_{3-x}\text{O}_4$ CSNs	19

Fig. 2.10 (a) XPS survey scan of PS type $\text{Co}_3\text{O}_4@\text{Mn}_x\text{Co}_{3-x}\text{O}_4$ CSNs; HR-XPS peak of (a) Co 2p _{3/2} , (b) Mn 2p _{3/2} and (c) O 1s	20
Fig. 2.11 (a) XPS survey scan of NP type $\text{Co}_3\text{O}_4@\text{Mn}_x\text{Co}_{3-x}\text{O}_4$ CSNs; HR-XPS peak of (a) Co 2p _{3/2} , (b) Mn 2p _{3/2} and (c) O 1s	21
Fig. 3.1 (a) A TEM image of 0.1 M PS type $\text{Co}_3\text{O}_4@\text{Mn}_x\text{Co}_{3-x}\text{O}_4$ CSNs; (b) Corresponding size distribution of 0.1 M PS type $\text{Co}_3\text{O}_4@\text{Mn}_x\text{Co}_{3-x}\text{O}_4$ CSNs	28
Fig. 3.2 (a) A HRTEM image of 0.1 M PS type $\text{Co}_3\text{O}_4@\text{Mn}_x\text{Co}_{3-x}\text{O}_4$ CSNs; (b) TEM-EDX of 0.1 M PS type $\text{Co}_3\text{O}_4@\text{Mn}_x\text{Co}_{3-x}\text{O}_4$ CSNs	29
Fig. 3.3 XRD pattern of 0.1 M PS type $\text{Co}_3\text{O}_4@\text{Mn}_x\text{Co}_{3-x}\text{O}_4$ CSNs.....	30
Fig. 3.4 (a) Survey scan of 0.1 M PS type $\text{Co}_3\text{O}_4@\text{Mn}_x\text{Co}_{3-x}\text{O}_4$ CSNs. High resolution XPS peak of (b) Co 2p _{3/2} , (c) Mn 2p _{3/2} , (c) O 1s	31
Fig. 3.5 (a) FC and ZFC hysteresis loop measured from 0.1 M PS type $\text{Co}_3\text{O}_4@\text{Mn}_x\text{Co}_{3-x}\text{O}_4$ CSNs at 5 K; the insets show enlarged views of M vs. H data. (b) FC and ZFC magnetization vs. temperature data of 0.1 M PS type $\text{Co}_3\text{O}_4@\text{Mn}_x\text{Co}_{3-x}\text{O}_4$ CSNs; the inset shows an enlarged view of M vs. T data. The FC and ZFC data were measured at an applied field of 300 Oe	33
Fig. 3.6 (a) Coercivity vs. temperature data, (b) exchange bias vs. temperature data of 0.1 M PS type $\text{Co}_3\text{O}_4@\text{Mn}_x\text{Co}_{3-x}\text{O}_4$ CSNs.....	33
Fig. 3.7 Field cooled hysteresis loops at different temperature from 5 K to 200 K of 0.1 M PS type $\text{Co}_3\text{O}_4@\text{Mn}_x\text{Co}_{3-x}\text{O}_4$ CSNs.....	34

CHAPTER 1: INTRODUCTION

Nanomaterials are a series of materials that are of sizeable interest in science, industrial engineering, and in technological and medical applications. Generally, the size of nanomaterials is from 1 nm to 100 nm in one or more dimension; subsequently they exhibit different properties from their corresponding bulk materials. Magnetic nanoparticles are a class of nanoparticles that can be manipulated using magnetic fields and that possess ordered magnetic spin structures. Consequently, magnetic nanomaterials can be utilized as magnetic storage devices, for energy harvesting and conversion and for biomedical engineering.

Core-shell nanoparticles (CSNs) have recently drawn considerable interest because of their physical and chemical properties that are strongly dependent on the structure of the core, shell, and interface. Generally core-shell nanoparticles have a nano scale core and a nano scale shell overlying the core to form multiple-structured nanomaterials. The important aspect of CSNs, especially for bimagnetic type, is the interaction between the core and shell and the tunability that is enabled through selection of material type, size, structural and morphological properties, etc. Novel functions and properties can be developed by tuning the composition of core-shell nanoparticles and the size of relative core shell regions. The magnetic core-shell nanoparticles are of considerable interest since their tunable nanostructure offers opportunities for establishing novel functions and properties for magnetic devices and other applications[1].

Bimagnetic CSNs, having distinct core and shell magnetic phases, are very actively being investigated for magnetic device and other applications[2].

Conventionally, bimagnetic core-shell nanoparticles (CSNs) possess a ferro/ferrimagnetic core and an antiferromagnetic shell. Inverted core-shell nanoparticles have been recently investigated, in which an antiferromagnetic (AFM) core and a ferromagnetic (FM) or ferrimagnetic (FiM) shell are used, due to their considerable tunability properties. It has been found that the magnetic properties of inverted core-shell nanoparticles, with special interest toward anisotropy, are enhanced with respect to their single phase counterparts[3]. The enhanced and sometimes novel magnetic properties of bimagnetic CSNs are highly promising for potential applications in magnetic random access memory, spintronic devices, cell separation, tissue engineering, drug delivery, MRI targeted-cell imaging, and hyperthermia[1, 4]. By tuning the size and the chemical composition of the core as well as the shell, nanomaterials can be produced with a variable properties that can play a significant role in various catalytic processes and offer sustainable solutions to current energy problems[5].

The exchange anisotropy or exchange bias (EB) occurs in a large variety of systems[6] which consist of an AFM phase that is in direct atomic contact with an FM or FiM phase. The EB effect is only manifested after the system is cooled below the respective Néel (T_N) and Curie (T_C) temperatures of the AFM and FM/FiM phases, respectively, in an applied external cooling field. It was first discovered by Meiklejohn and Bean in fine Co particles covered by CoO more than 60 years ago[7]. The exchange bias is the phenomenon in which the hysteresis loop is shifted along the magnetic field axis either in the positive direction or negative direction, although shifts can also be

manifested along the magnetization (M) axis. Bimagnetic core-shell nanoparticles have distinguishable magnetic structure between the core region and the shell region; consequently, studies of the exchange bias effect in bimagnetic core-shell nanomaterials have grown in number rapidly and are still very active today.

Fig. 1.1 shows a classic model of exchange bias phenomenon. Exchange bias arises between two different magnetic structure bilayers: generally it occurs at the interface between an antiferromagnetic layer and a ferromagnetic or ferrimagnetic layer. The hard magnetization of the AFM bias controls the magnetization of softer FM/FiM layer[6, 9]. When the AFM and FM/FiM structured interface system is cooled in an applied external magnetic field through the temperature T_N , the AFM spin and FM/FiM spin pairs interact with each other and can be robustly pinned so that the spins of the FM/FiM layer (at the interface) are aligned in a specific direction which biases its magnetization. Subsequently, the hysteresis loop is shifted to either positive field direction or negative field direction instead centered at zero field. This exchange bias field H_{EB} is illustrated in Fig. 1.1[8]. The exchange bias can be calculated based on the formula $H_e = |H_{ZFC+} - H_{FC+} - H_{FC-} + H_{ZFC-}|/2$ where the +/- indicate positive/negative H values when $M=0$.

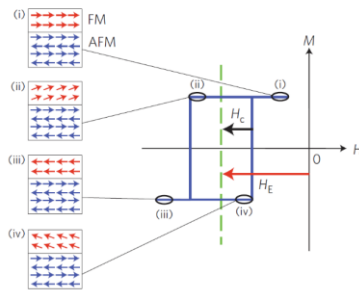


Fig. 1.1 Classic model of exchange bias phenomenon. Magnetization vs. field hysteresis loop is shifted along the field axis at $T < T_N$ [8].

A substantial amount of previous work on exchange bias has been done on different systems, such as gold-coated magnetic core-shell nanoparticles[10–12], transition metal and transition metal oxide core-shell nanoparticles[13–16]. The study of the exchange bias in bimagnetic and inverted core-shell nanoparticles is still ongoing particularly in the context of obtaining a fuller understanding of the mechanism of the effect.

The mixed-valence cobalt oxide (Co_3O_4) nanoparticles are widely utilized in lithium-ion batteries[17, 18], gas sensing[19] and heterogeneous catalysis applications[20]. Cobalt oxide has a normal spinel structure with Co^{2+} ions occupying tetrahedral sites whereas Co^{3+} ions occupying octahedral sites (see Fig. 1.2), for which the magnetic moment is derived from Co^{2+} ions whereas Co^{3+} ions are nonmagnetic[21]. Bulk Co_3O_4 has a Néel temperature of 40 K. When the temperature of the sample is above the Néel temperature, the magnetic ordering of the antiferromagnetic spin structure will be destroyed by thermal energy so that it becomes paramagnetic.

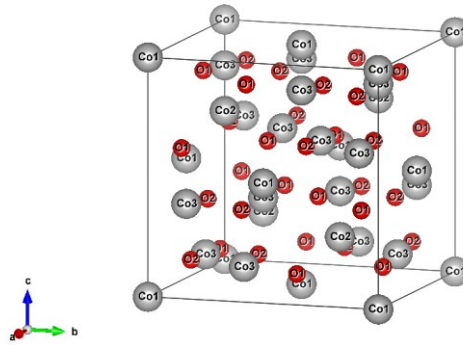


Fig. 1.2 Normal spinel structure of cobalt oxide (Co_3O_4).

Previous studies in our lab showed that the magnetic properties of a series of Cr_2O_3 based CSNs, that were synthesized hydrothermally, are tunable in terms of coercivity and exchange bias. Hence, in order to find whether this synthesis approach also can be applied to a different transition metal oxide nanoparticles system, I made an investigation of Co_3O_4 based core-shell nanoparticles along two different directions: in the first part, the shape dependence of different morphologies of Co_3O_4 based $\text{Mn}_x\text{Co}_{3-x}\text{O}_4$ core-shell nanoparticles were investigated whereas in the second part, the effect of Mn concentration dependence on the structure and magnetic properties of Co_3O_4 based $\text{Mn}_x\text{Co}_{3-x}\text{O}_4$ core-shell nanoparticles was studied.

There are two hypotheses that apply to my study: Is it possible to incorporate Mn ions into the tetrahedral sites of the spinel structure of a Co_3O_4 -based shell (Fig. 1.3) grown using a hydrothermal nanophase epitaxy method? Can different morphologies of $\text{Co}_3\text{O}_4@\text{Mn}_x\text{Co}_{3-x}\text{O}_4$ core-shell nanoparticles be synthesized by adjustment of the pH value of the aqueous fluid?

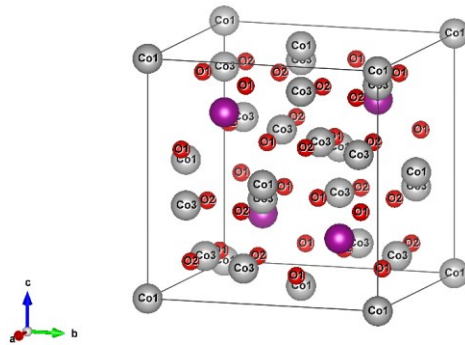


Fig. 1.3. The hypothetical structure of $\text{Co}_3\text{O}_4@\text{Mn}_x\text{Co}_{3-x}\text{O}_4$ core-shell nanoparticles. The purple circles are Mn ions incorporated in tetrahedral sites.

In order to confirm these two hypotheses, X-ray diffraction (XRD), scanning electron microscopy (SEM), transmission electron microscopy (TEM), energy-dispersive X-ray analysis (EDX), X-ray photoelectron spectroscopy (XPS), and superconducting quantum interface device (SQUID) magnetometry were utilized to investigate the morphologies, structure and magnetic properties of CSNs.

CHAPTER 2: A STUDY OF DIFFERENT MORPHOLOGIES OF MANGANESE INCORPORATED CORE-SHELL NANOPARTICLES

Abstract

The mixed-valence oxide Co_3O_4 nanoparticles, having the normal spinel structure, possess large surface area, active-site surface adsorption properties, and fast ion diffusivities. Consequently, they are widely used in lithium-ion batteries, as well as for gas sensing and heterogeneous catalysis applications. In our research, we use a two-step method to synthesize Co_3O_4 -based core-shell nanoparticles (CSNs). Cobalt oxide (Co_3O_4) nanoparticles were successfully synthesized using a wet synthesis method employing KOH and cobalt acetate. Manganese was incorporated into the Co_3O_4 structure to synthesize inverted $\text{Co}_3\text{O}_4@\text{Mn}_x\text{Co}_{3-x}\text{O}_4$ CSNs using a hydrothermal method. By adjustment of pH value, we obtained two different morphologies of CSNs, one resulting in pseudo-spherical and octahedron-shaped nanoparticles (PS type) whereas the second type predominantly have a nanoplate (NP type) morphology. X-ray diffraction (XRD), scanning electron microscopy (SEM), transmission electron microscopy (TEM), and x-ray photoelectron spectroscopy (XPS) have been performed in order to determine the morphological and structural properties of our CSNs, whereas the magnetic properties have been characterized using a superconducting quantum interference device (SQUID) magnetometer. XRD and TEM results show that the CSNs have the same spinel crystal structure throughout the core and shell with an average particle size of ~ 19.8 nm. Our Co_3O_4 nanoparticles, as measured prior to CSN formation, are shown to be antiferromagnetic (AFM) in nature as shown by the magnetization data. Our SQUID data

indicate that the core-shell nanoparticles have both AFM (due to the Co_3O_4 core) and ferrimagnetic properties (of the shell) with a coercivity field of 300 Oe and 150 Oe at 5 K for the PS and NP samples, respectively. The magnetization vs temperature data show a spin order-disorder transition at ~ 33 K and a superparamagnetic blocking temperature of ~ 90 K for both batches.

Introduction

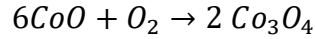
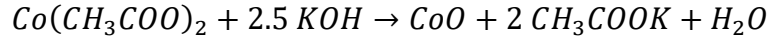
Core-shell nanoparticles (CSNs) have drawn much attentions due to their finite-size dependent magnetic properties and because of their technological applications [1,2]. Bimagnetic CSNs, which have distinct core and shell magnetic properties, are being explored for magnetic devices, medicals and other applications [3]. The mixed-valence oxide Co_3O_4 nanoparticles, having the normal spinel structure, possess large surface area, active-site surface adsorption properties, and fast ion diffusivities. Consequently, they are widely used in lithium-ion batteries [4,5], as well as for gas sensing [6] and heterogeneous catalysis applications [7]. Co_3O_4 has an ordered structure in the normal spinel phase with Co^{2+} ions occupying tetrahedral sites whereas the Co^{3+} ions occupy octahedral sites, for which the magnetic moment is derived from the Co^{2+} ions whereas Co^{3+} ions are nonmagnetic [8]. Bulk Co_3O_4 is antiferromagnetic in nature with a Néel temperature of 40 K. The shape-dependent exchange bias properties of bimagnetic nanostructured materials have drawn much interest from the scientific community. Fan et al. have studied the magnetic properties of urchin-like $\text{Co}_3\text{O}_4/\text{CoFe}_2\text{O}_4$ nanocomposites and claim that the mismatched surface spin in the hetero-structured $\text{Co}_3\text{O}_4/\text{CoFe}_2\text{O}_4$ nanocomposites are greatly reduced [9]. Chen et al have shown that octahedral Co_3O_4

nanoparticles exhibit an antiferromagnetic phase transition at a Néel temperature of ~ 10 K and much of the Co^{3+} ions are in the high-spin state[10]. Teng et al studied face-raised Co_3O_4 nano-octahedral shaped nanomaterials and found that they have a higher remanence and saturation magnetization compared to normal Co_3O_4 octahedral nanomaterials[11]. It is still unclear as to how the exchange bias effect is dependent upon the geometry of Co_3O_4 -based bimagnetic nanostructures. Herein we used our hydrothermal nanophase epitaxy (HNE) method [12,13] to prepare $\text{Co}_3\text{O}_4@\text{Mn}_x\text{Co}_{3-x}\text{O}_4$ inverted CSNs with two different morphologies for the first time, and addressed the question as to how the magnetic properties depend upon their shape. Our bimagnetic CSNs were characterized using X-ray diffraction (XRD), scanning electron microscopy (SEM), transmission electron microscopy (TEM) and a SQUID magnetometry.

Experimental

Co_3O_4 nanoparticles were synthesized using a soft chemical approach [14]. A quantity of 0.04 M cobalt acetate was mixed with 0.1M potassium hydroxide aqueous solution to be used as a precursor. Next, we used hydrochloric acid and potassium hydroxide to adjust the pH value of the precursor solution to make two batches: one with a pH value of 9.5 (PS precursor solution) and another with a pH value of 8.5 (NP precursor solution). Both solutions were stirred for 2 hours at room temperature. Next, the solutions were refluxed in a water bath at 100°C for 4 hours. After centrifugation, the residue was rinsed thoroughly using 50% ethanol solutions, and allowed to dry at room temperature. The resulting dark grey PS and NP powders were calcined at 450°C and 550°C in air for 4 hours, respectively. For both samples, we obtained black powder. The

possible chemical reactions that result in the formation of Co_3O_4 nanoparticles are shown below:



The Co_3O_4 nanoparticles were subsequently used to synthesize Co_3O_4 based $\text{Mn}_x\text{Co}_{3-x}\text{O}_4$ inverted core-shell nanoparticles using our hydrothermal Nano phase epitaxy (HNE) method³. For each type of sample, 20 ml distilled water was deoxidized with dry nitrogen gas for 20 minutes at room temperature. Subsequently, 0.176 g of MnCl_2 were dissolved and sonicated in the aqueous solution for 10 minutes. Hydrochloric acid was used to control the pH value to a value of the MnCl_2 solution close to 3.5, which was subsequently mixed with 0.337 g of PS or NP Co_3O_4 nanoparticles. The nanoparticle-solution mixture was first sonicated 30 minutes at room temperature and then transferred to an autoclave, where it was hydrothermally treated at 200 °C for 30 hours. The resulting core-shell nanoparticles (CSN) residue was subsequently rinsed using distilled water several times, centrifuged and dried at room temperature overnight. The pH value and calcination temperature differences between two types CSNs can be seen in Table 2.1.

Table 2.1 Experimental parameters of two different morphologies CSNs

Samples	pH value before refluxing	Hydrothermal time (hours)	Calcination temperature for Co_3O_4(°C)
PS type CSNs	9.5	30	450
NP type CSNs	8.5	30	550

Characterization

An FEI Quanta 200 scanning electron microscopy (SEM) was used for SEM images and energy dispersive x-ray spectroscopy (EDS). First, we dissolved 5 mg powdered samples in ethanol and sonicated the solution for 10 minutes; Then a pipette transfer gun was used and put 2~3 drops on a cleaned copper tape. SEM images were taken at 20 KV beam voltage and kept the imaging distance at 6mm, gun-to-sample EDX distance was kept at 10 mm. In order to minimize charging effects, a short piece copper tape was used connecting the surface and the bottom portion of the aluminum stage.

The morphology of nanoparticles was gained by an FEI Titan 80-300 Transmission Electron Microscopy with an operating voltage of 300 KeV. The average particle size was given by low resolution TEM images using ImageJ software.

The oxidation states of the cation ions and the composition of CSNs were gained by XPS measurements. A Versa Probe XPS from Physical Electronics was used to gain this. X-ray source is monochromated K alpha rays from aluminum at 1486 eV, 117.4 eV pass energy was used for surveys and about 58.7 eV or below pass energy was used for high-resolution scans. XPS data analysis and peak fitting were performed by using CasaXPS 2.3.16 software, carbon 1s peak (284.8 eV) from carbon tape was used for energy calibration.

The background of the collected data was modeled by Shirley function, while for high resolution data peak fitting, a GL (30) function was used for symmetry peaking fitting and a LA (2, 2.8, 18) function was used for asymmetry peaking fitting. GL (p) means Gaussian/Lorentzian product formula where the mixing is determined by $m = p/100$, GL (100) is a pure Lorentzian while GL (0) is pure Gaussian. LA (α , β , m) means

asymmetric line-shape where α and β define the spread of the tail on either side of the Lorentzian component. The parameter m specifies the width of the Gaussian used to convolute the Lorentzian curve. In each of survey spectra, the main peaks can be clearly indexed to Co 2p, O 1s, C 1s and Mn 2p regions, which mean that there are no impurity components presented.

Hysteresis and magnetization vs temperature measurements were characterized by a Quantum Design SQUID MPMS/XL magnetometer. Magnetic hysteresis measurements and magnetization vs temperature measurements were performed in both field cooled and zero field cooled conditions. A soft gel capsule was used to load powder samples to the magnetometer, the temperature of both FC and ZFC measurements first was raised to 300 K and then gradually down to 5 K; For FC hysteresis measurements, 20 KOe magnetic field was applied whereas for ZFC measurements, there is no applied magnetic field. The magnetization vs field data were gained in the range from -10 K Oe to +10 K Oe. FC and ZFC magnetization vs temperature data were taken in the range from 5 K to 300 K with an applied 300 Oe magnetic field.

The nanoparticles powder was characterized by a Bruker, D8 Discover X-ray Diffraction machine with Cu-K α radiation (wavelength 1.54 Å) over the 2θ range 10 to 90°. Disperse a small amount of powder samples on a glass slide, use ethanol to adhere them together. Then fix the sample slide to a vertical aluminum stage and ready to be scanned. All measurements were under room temperature.

Results and Discussion

Fig. 2.1 shows the SEM images of PS type and NP type Co₃O₄ nanoparticles: we observed that our PS type Co₃O₄ nanoparticles (NPs) are pseudo-spherical and

octahedron-shaped (Fig. 2.1(a)), whereas our NP type Co_3O_4 nanoparticles, which predominantly have a nanoplate morphology (Fig. 2.1 (b)). Fig. 2.2 (a), which shows a TEM image of PS type $\text{Mn}_x\text{Co}_{3-x}\text{O}_4$ CSNs, indicated that there was no change in shape after manganese ions incorporated in the formation of our $\text{Co}_3\text{O}_4@\text{Mn}_x\text{Co}_{3-x}\text{O}_4$ CSNs. A histogram plot of the size distribution of the PS type $\text{Co}_3\text{O}_4@\text{Mn}_x\text{Co}_{3-x}\text{O}_4$ CSNs is shown in Fig. 2.2 (b), from which we obtained an average size of 19.8 nm. Fig. 2.3 (a) shows a TEM image of NP type $\text{Mn}_x\text{Co}_{3-x}\text{O}_4$ CSNs, indicated that there was no change in shape after manganese ions incorporated in the formation of our $\text{Co}_3\text{O}_4@\text{Mn}_x\text{Co}_{3-x}\text{O}_4$ CSNs. The diameter and thickness of the NP type CSNs we estimated were 188.7 nm and 9 nm, respectively (Fig. 2.3 (b) and (c)). a HRTEM image of the PS type CSNs, where the core and the shell regions can be easily distinguished by the interface as indicated in the image; and the shape of the isolated particle strongly support our SEM results of PS type Co_3O_4 nanoparticles which means the hydrothermal treatment doesn't change the shape of PS type Co_3O_4 nanoparticles; The approximate thickness of the shell region from the HRTEM images is ~ 1.3 nm. SEM-EDS and TEM-EDS results indicated the presence of manganese in the CSNs. The same crystallographic symmetry and atomic plane continuity from core to shell, due to epitaxial growth of the shell over the core, of the CSNs is seen from our TEM results.

Fig. 2.5 shows that the X-ray diffraction patterns of both morphologies of $\text{Mn}_x\text{Co}_3\text{O}_4$ CSNs measured at room temperature. It is conspicuous that both of the morphologies of nanoparticles maintain the same spinel structure. This is evident from the analysis of XRD patterns measured from Co_3O_4 NPs and $\text{Co}_3\text{O}_4@\text{Mn}_x\text{Co}_{3-x}\text{O}_4$ CSNs,

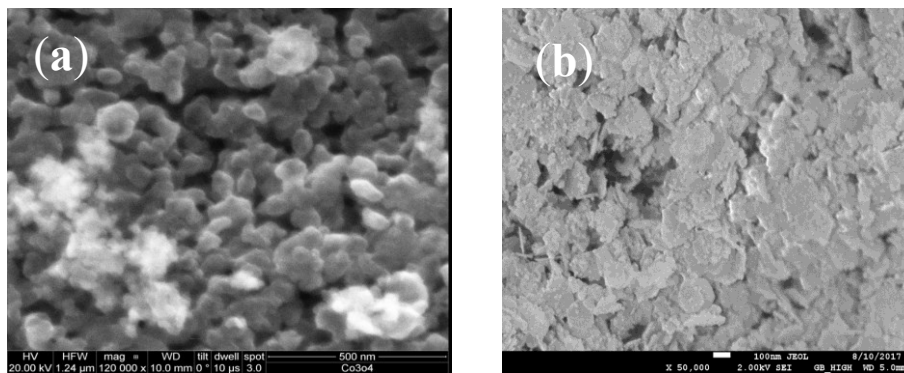


Fig. 2.1 (a) A SEM image of the PS type Co_3O_4 nanoparticles; (b) a SEM image of the NP type Co_3O_4 nanoparticles.

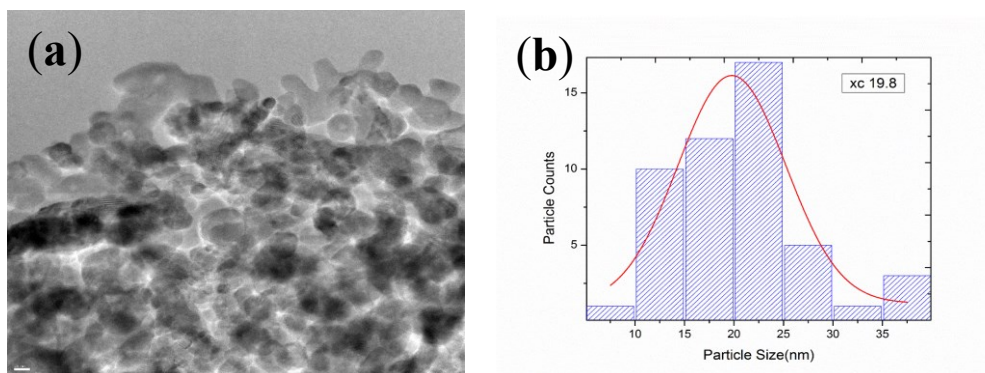


Fig. 2.2 (a) a TEM image of the PS type $\text{Co}_3\text{O}_4@Mn_x\text{Co}_{3-x}\text{O}_4$ CSNs; (b) Corresponding Size distribution of the PS type $\text{Co}_3\text{O}_4@Mn_x\text{Co}_{3-x}\text{O}_4$ CSNs.

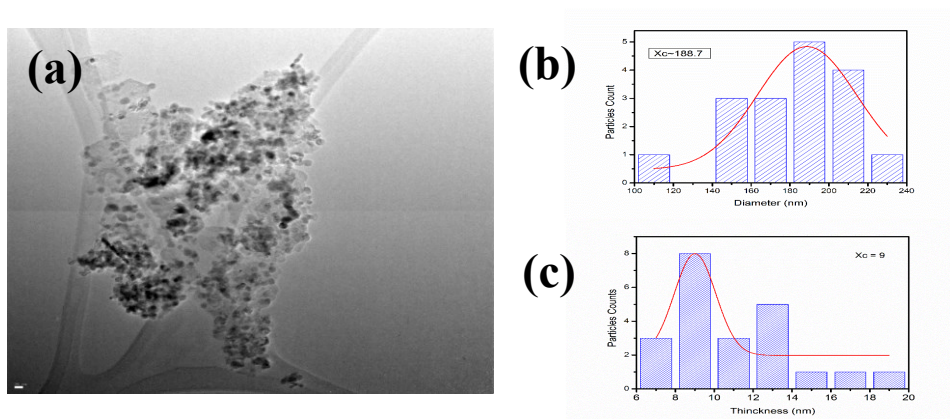


Fig. 2.3 (a) a TEM image of the NP type $\text{Co}_3\text{O}_4@Mn_x\text{Co}_{3-x}\text{O}_4$ CSNs; (b) Corresponding diameter distribution of the NP type $\text{Co}_3\text{O}_4@Mn_x\text{Co}_{3-x}\text{O}_4$ CSNs; (c) Corresponding thickness distribution of the NP type $\text{Co}_3\text{O}_4@Mn_x\text{Co}_{3-x}\text{O}_4$ CSNs.

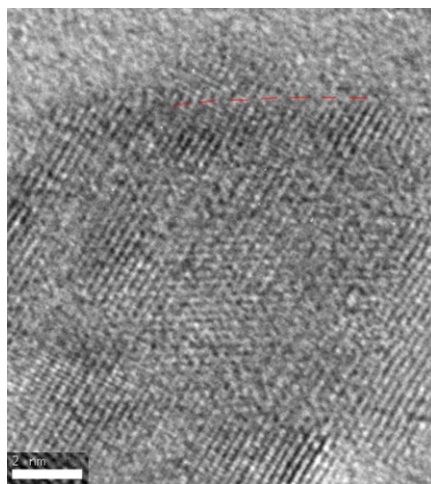


Fig. 2.4 A high-resolution TEM image of PS type $\text{Co}_3\text{O}_4@\text{Mn}_x\text{Co}_{3-x}\text{O}_4$ CSNs.

which yielded structures having the same $F\bar{4}3m$ symmetry for all NPs and CSNs of the study. Furthermore, we do not find any evidence for impurity phases (e.g., MnO) in the nanoparticles from the XRD data. Since the difference of the ionic radii between Mn^{2+} and Co^{2+} is small[15], Mn^{2+} ions can easily replace Co^{2+} ions with minimal distortion of the spinel crystal structure of Co_3O_4 . The average crystallite size of PS Co_3O_4 nanoparticles calculated using Scherrer equation was found to be 17.30(2) nm whereas the size of PS type $\text{Co}_3\text{O}_4@\text{Mn}_x\text{Co}_{3-x}\text{O}_4$ CSNs determined by using the same method was found to be 19.40(3) nm. The latter result is consistent with the results of particle size distribution calculated from our TEM images. Thus, the growth in nanoparticles shows that Mn incorporation in the shell region with a thickness of 1.1-1.3 nm. Conversely, for the NP type CSNs, our preliminary result showed that the average crystallite size for the NP type Co_3O_4 nanoparticles is 13.2(4) nm and for the NP type CSNs the size is 21.4(2) nm, as obtained using the Scherrer equation in the analysis of XRD data. In order to further evaluate the structural properties of CSNs, Rietveld refinement was made of the

XRD data. The space group symmetry of $F\bar{4}3m$ structure was used with the starting parameters for the Co^{2+} ions at the unit cell positions $x = \frac{1}{4}$, $y = \frac{1}{4}$ and $z = \frac{1}{4}$. A second $F\bar{4}3m$ CIF file was added in order to account for the shell region in the refinement. Our fitting results show consistently that the goodness-of-fit is improved significantly by use of a core-shell structure model as opposed to a single structure model. The lattice parameters of core region and shell region were found to be $8.08(0.4) \text{ \AA}$ and $8.12(2) \text{ \AA}$ respectively; this slight expansion of the lattice parameter is consistent with the Shannon ionic radius of the high spin Mn^{2+} ion (0.66 \AA) being slightly larger than that of high-spin Co^{2+} ion (0.58 \AA) and the former partially substituting for the latter in the tetrahedral sites for the PS type CSNs, of the spinel structure in the shell region.

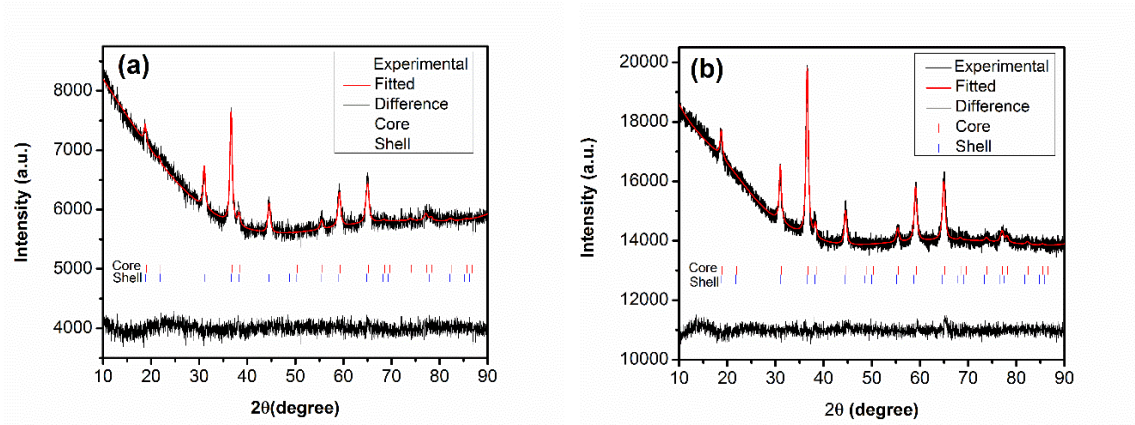


Fig. 2.5 XRD patterns of $\text{Co}_3\text{O}_4@\text{Mn}_x\text{Co}_{3-x}\text{O}_4$ CSNs: (a) PS type $\text{Co}_3\text{O}_4@\text{Mn}_x\text{Co}_{3-x}\text{O}_4$ CSNs; (b) NP type $\text{Co}_3\text{O}_4@\text{Mn}_x\text{Co}_{3-x}\text{O}_4$ CSNs.

Fig. 2.6 and Fig. 2.7 shows magnetic measurement data of PS type and NP type $\text{Co}_3\text{O}_4@\text{Mn}_x\text{Co}_{3-x}\text{O}_4$ CSNs. Fig. 2.6 (a) shows the field cooled (FC) and zero field cooled (ZFC) hysteresis loops measure from PS type $\text{Co}_3\text{O}_4@\text{Mn}_x\text{Co}_{3-x}\text{O}_4$ CSNs at 5 K, Fig. 2.6 (b) shows the field cooled (FC) and zero field cooled (ZFC) hysteresis loops measure

from NP type $\text{Co}_3\text{O}_4@\text{Mn}_x\text{Co}_{3-x}\text{O}_4$ CSNs at 5 K, whereas the insets show enlarged views of the M vs H data measured at 5 K. The coercivity shown in the FC hysteresis loop for the PS type $\text{Co}_3\text{O}_4@\text{Mn}_x\text{Co}_{3-x}\text{O}_4$ CSNs is ~ 300 Oe whereas the coercivity for the NP type $\text{Co}_3\text{O}_4@\text{Mn}_x\text{Co}_{3-x}\text{O}_4$ CSNs is ~ 150 Oe. In addition to the greater coercivity, the data displayed in Fig. 2.6 show that the PS type CSNs exhibit a much less drastic change in slope of the magnetization upon reversal from H field, either from + to - values or from - to + field, than do the NP type CSNs. The FC magnetization saturation values for the PS type and NP type CSNs at 5 K is approximately 0.11 emu/g and 0.095 emu/g, respectively. The FC vs zero field cooled (ZFC) hysteresis loops do not show significant shifts either in the negative and positive H axis directions. The exchange bias was calculated based on the formula $H_e = |H_{ZFC+} - H_{FC+} - H_{FC-} + H_{ZFC-}|/2$ where the +/- indicate positive/negative H values when M=0. The exchange bias for PS type CSNs was ~ 33 Oe whereas for the NP type CSNs it was 31 Oe, as measured at 5 K. Our magnetometry data show that our Co_3O_4 nanoparticles and the core regions of the CSNs are antiferromagnetic, whereas the Mn-substituted Co_3O_4 ($\text{Mn}_x\text{Co}_{3-x}\text{O}_4$) spinel phase of the shell region is ferrimagnetic. Thus, our CSNs have the inverted core-shell magnetic configuration. Fig. 2.7 (a) and (b) show FC and ZFC magnetization vs temperature data measured from our PS type and NP type CSNs in the range from 5 to 300 K, respectively. These data show a spin order-disorder transition at ~ 33 K and a superparamagnetic blocking temperature of ~ 90 K for both types of CSNs. The spin order-disorder transition peaked feature appears to be more prominent in the magnetization vs temperature data of the NP type CSNs than that of the PS type CSNs.

Fig. 2.10 (a) and Fig. 2.11 (a) show survey scans of PS type and NP type $\text{Co}_3\text{O}_4@\text{Mn}_x\text{Co}_{3-x}\text{O}_4$ CSNs. The presence of Mn is strongly supported from our SEM-EDX, TEM-EDX and XRD results, which indicate that Mn was successfully incorporated

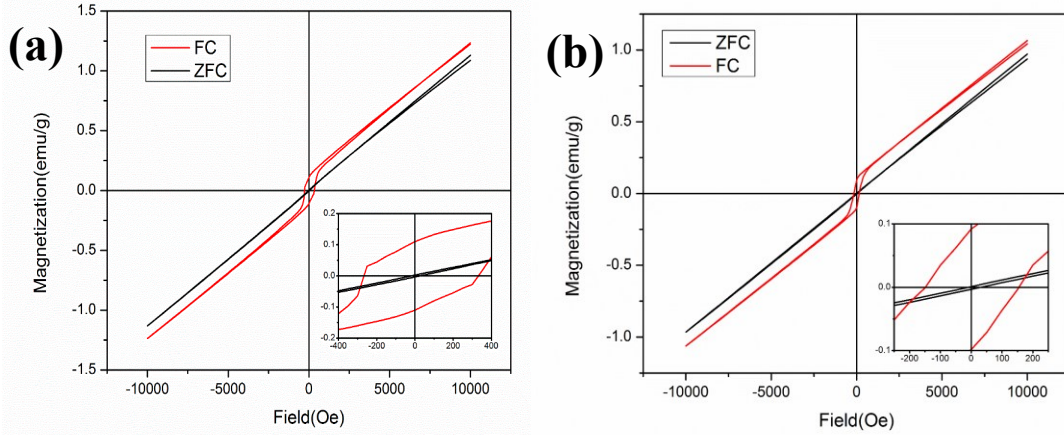


Fig. 2.6: (a) FC and ZFC hysteresis loops measured from PS type $\text{Co}_3\text{O}_4@\text{Mn}_x\text{Co}_{3-x}\text{O}_4$ CSNs at 5 K; (b) FC and ZFC hysteresis loops measured from NP type $\text{Co}_3\text{O}_4@\text{Mn}_x\text{Co}_{3-x}\text{O}_4$ CSNs at 5 K; the insets show enlarged views of the M vs H data.

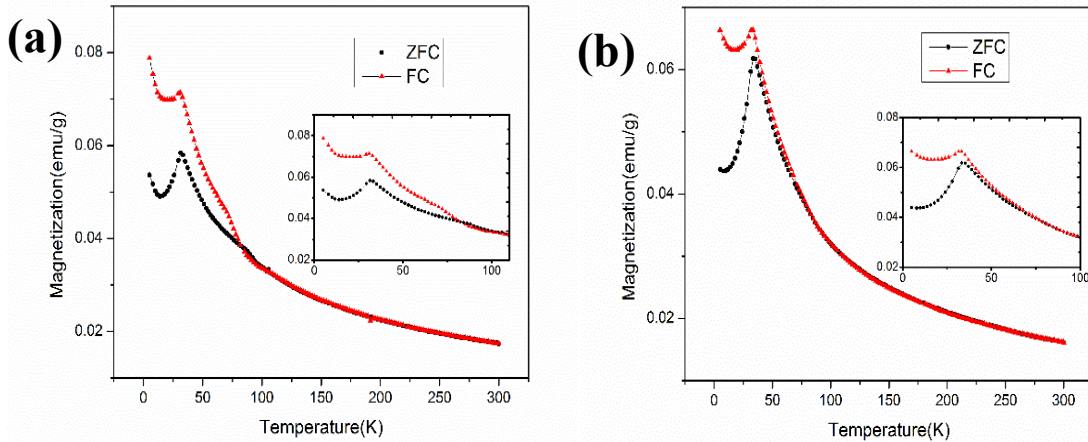


Fig. 2.7: (a) FC and ZFC magnetization vs. temperature data of PS type $\text{Co}_3\text{O}_4@\text{Mn}_x\text{Co}_{3-x}\text{O}_4$ CSNs; (b) FC and ZFC magnetization vs. temperature data of NP type $\text{Co}_3\text{O}_4@\text{Mn}_x\text{Co}_{3-x}\text{O}_4$ CSNs; the insets show enlarged views of M vs. T data. The FC and ZFC data were measured at an applied field of 300 Oe. The FC hysteresis measurements were made with the samples cooled from 300 K to 5 K at 20,000 Oe

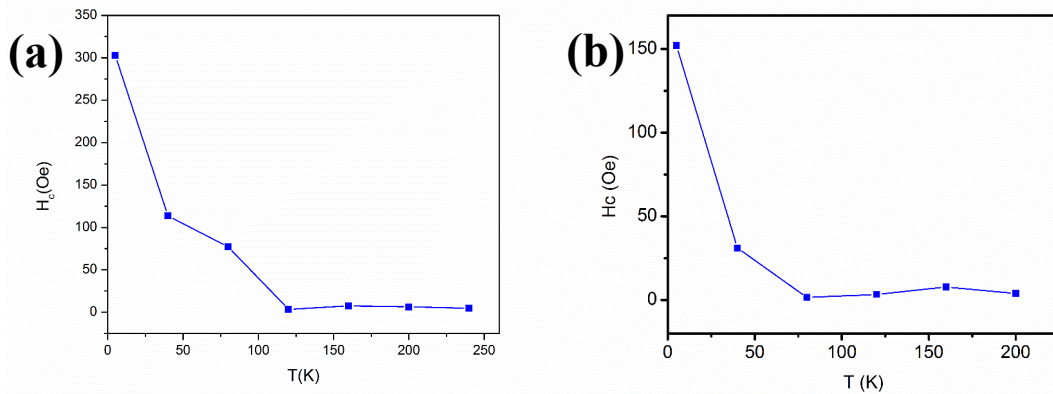


Fig. 2.8 Coercivity vs. temperature data of: (a) NP type $\text{Co}_3\text{O}_4@\text{Mn}_x\text{Co}_{3-x}\text{O}_4$ CSNs, (b) PS type $\text{Co}_3\text{O}_4@\text{Mn}_x\text{Co}_{3-x}\text{O}_4$ CSNs.

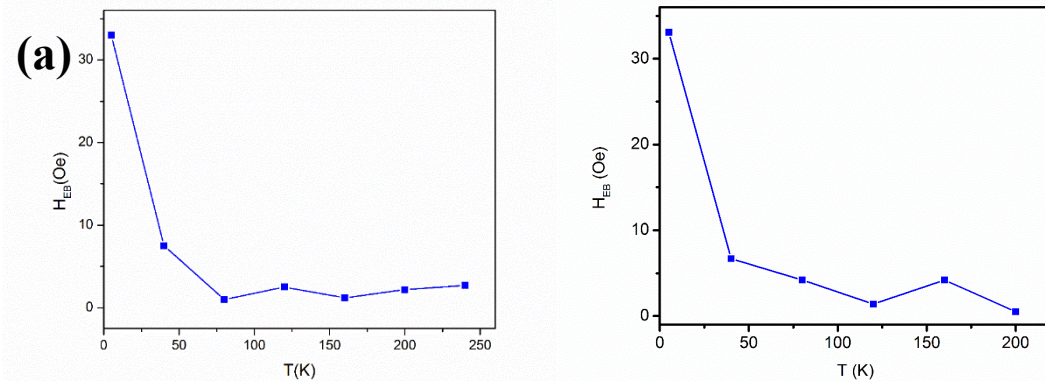


Fig. 2.9 Exchange Bias vs. temperature data of: (a) NP type $\text{Co}_3\text{O}_4@\text{Mn}_x\text{Co}_{3-x}\text{O}_4$ CSNs, (b) PS type $\text{Co}_3\text{O}_4@\text{Mn}_x\text{Co}_{3-x}\text{O}_4$ CSNs.

in the spinel structure of Co_3O_4 . The Mn atomic weights of PS type and NP type are 5.31 at% and 2.98 at% as obtained from XPS survey spectra, respectively. High resolution XPS data show that the oxidation states of Cobalt ions are Co^{2+} and Co^{3+} whereas oxidation of manganese is Mn^{2+} only (Fig. 2.10 (c) and Fig. 2.11 (c)), which indicates that Mn was incorporated into the tetrahedral site of the spinel structure of Co_3O_4 and therefore successfully replaced Co^{2+} ions. Detailed analysis showed that there are three different types of Co binding: one is Cobalt (III) bonded with oxygen (Co (III)-O), one is Cobalt (II) bonded with oxygen (Co (II)-O), and the other one is bonded with hydroxyl

ion (Co-OH) (see Fig. 2.10 (b) and Fig. 2.11 (b)). Quantitative analysis of our high resolution XPS Mn 2p_{3/2}, Co 2p 3/2 and O 1s peaks (see reference 3 for further details on the procedures) yields a concentration of 5.31 Mn at% in the shell region of the PS type Mn_xCo_{3-x}O₄ CSNs and 2.98 Mn at% in the shell region of the NP type Mn_xCo_{3-x}O₄ CSNs, respectively (see Table 2.2). Thus, from stoichiometry calculations we estimate a chemical formula for the PS type to be Co₃O₄@Mn_{0.84}Co_{2.16}O_{3.92} CSNs.

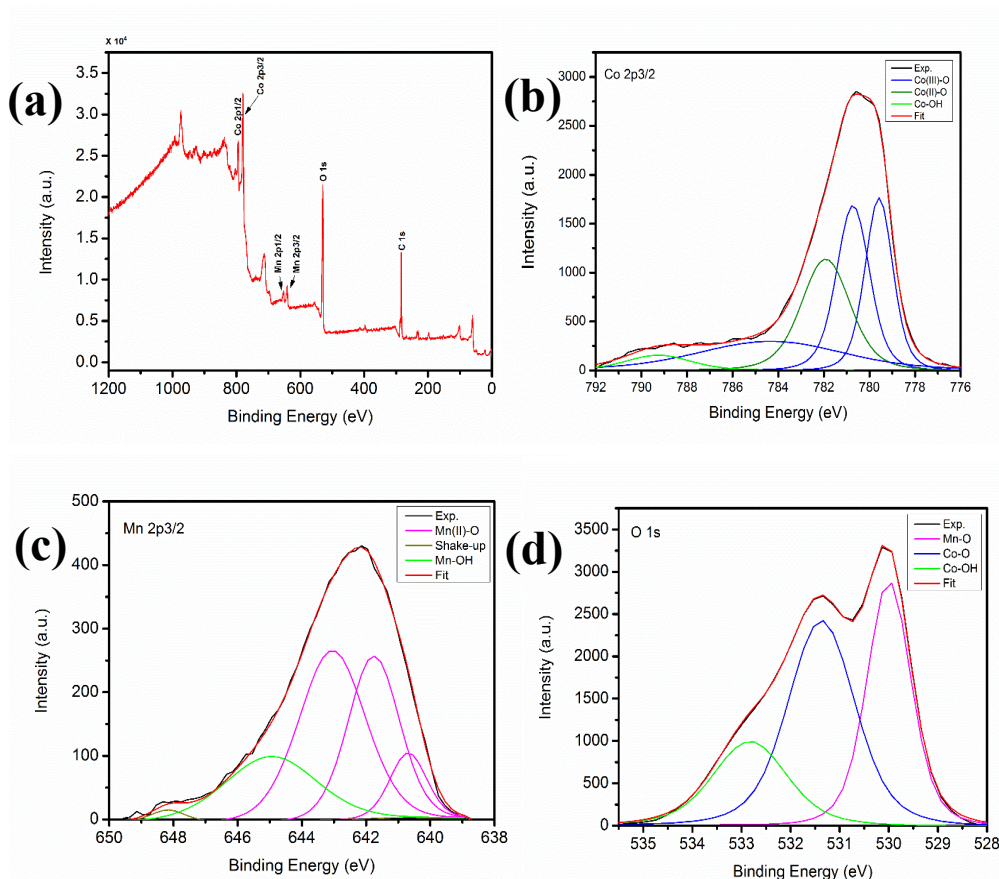


Fig. 2.10 (a) XPS survey scan of PS type Co₃O₄@Mn_xCo_{3-x}O₄ CSNs; HR-XPS peak of (a) Co 2p_{3/2}, (b) Mn 2p_{3/2} and (c) O 1s.

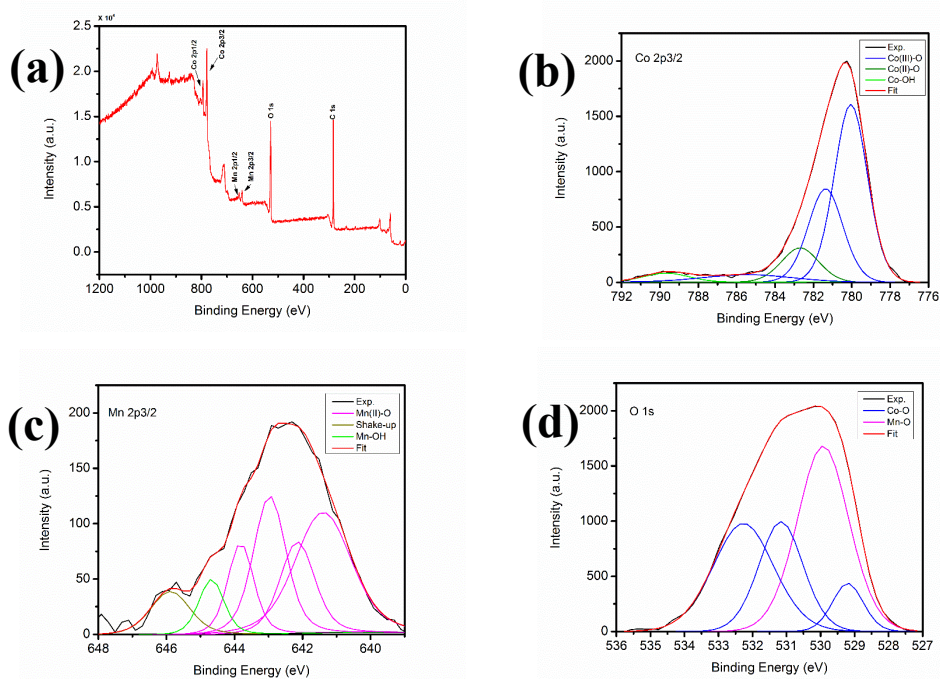


Fig. 2.11 (a) XPS survey scan of NP type $\text{Co}_3\text{O}_4@\text{Mn}_x\text{Co}_{3-x}\text{O}_4$ CSNs; HR-XPS peak of (a) Co 2p_{3/2}, (b) Mn 2p_{3/2} and (c) O 1s.

Table 2.2 Chemical composition obtained from XPS data

Samples	Mn At %	Co At %	O At %
PS type CSNs	5.31	30.51	64.18
NP type CSNs	2.98	25.66	71.36

Conclusions

We have successfully synthesized two different morphologies of $\text{Co}_3\text{O}_4@\text{Mn}_x\text{Co}_{3-x}\text{O}_4$ CSNs by using a two-step synthesis process, the first involving a soft chemical approach and the second our HNE method to develop the core-shell nanostructure. By adjustment of the pH value in the first step of the synthesis, we were able to grow CSNs having either a pseudo-spherical and octahedron-like shapes (PS) or nanoplate morphology (NP). Our characterization results confirmed that manganese ions

were incorporated into the shell region of both the PS type and NP type CSNs. Our TEM results explicitly show that both two different morphologies have an explicitly core-shell structure and epitaxial registry of shell layers on core atomic layers. The XRD results confirm that both the core region and shell region of PS type and NP type CSNs have the spinel structure with $F\bar{4}3m$ symmetry. Our XPS results show that oxidation state of manganese is Mn^{2+} only and no other oxidation states were found. An estimated chemical formula for the PS type CSNs is $Co_3O_4@Mn_{0.84}Co_{2.16}O_{3.92}$. Our SQUID magnetometry data confirm that our CSNs have the inverted magnetic configuration with an AFM core and FiM shell.

References

1. Cabuil, V., Dupuis, V., Talbot, D., & Neveu, S. (2011). Ionic magnetic fluid based on cobalt ferrite nanoparticles: Influence of hydrothermal treatment on the nanoparticle size. *Journal of Magnetism and Magnetic Materials*, 323(10), 1238–1241.
2. Schmidt, W. (2009). Solid catalysts on the nanoscale: design of complex morphologies and pore structures. *ChemCatChem*, 1(1), 53-67.
3. Hossain, M. D., Mayanovic, R. A., Sakidja, R., Benamara, M., & Wirth, R. (2018). Magnetic properties of core-shell nanoparticles possessing a novel Fe (II)-chromia phase: an experimental and theoretical approach. *Nanoscale*.
4. Lou, X. W., Deng, D., Lee, J. Y., & Archer, L. A. (2008). Thermal formation of mesoporous single-crystal Co_3O_4 nano-needles and their lithium storage properties. *Journal of materials chemistry*, 18(37), 4397-4401.
5. Wang, X., Tian, W., Zhai, T., Zhi, C., Bando, Y., & Golberg, D. (2012). Cobalt (II, III) oxide hollow structures: fabrication, properties and applications. *Journal of Materials Chemistry*, 22(44), 23310-23326.
6. Li, W. Y., Xu, L. N., & Chen, J. (2005). Co_3O_4 nanomaterials in lithium-ion batteries and gas sensors. *Advanced Functional Materials*, 15(5), 851-857.

7. Xie, X., Li, Y., Liu, Z. Q., Haruta, M., & Shen, W. (2009). Low-temperature oxidation of CO catalysed by Co₃O₄ nanorods. *Nature*, 458(7239), 746.
8. Roth, W. L. (1964). Magnetic properties of normal spinels with only AA interactions. *Journal de Physique*, 25(5), 507-515.
9. Fan, S., Wang, W., Ke, H., Rao, J. C., & Zhou, Y. (2016). Bimagnetic urchin-like Co₃O₄/CoFe₂O₄ nanocomposites: synthesis and magnetic properties. *RSC Advances*, 6(99), 97055-97062.
10. Chen, Y. H., Zhou, J. F., Mullarkey, D., O'Connell, R., Schmitt, W., Venkatesan, M., & Zhang, H. Z. (2015). Synthesis, characterization and magnetic properties of ultrafine Co₃O₄ octahedra. *AIP Advances*, 5(8), 087122.
11. Teng, Y., Song, L. X., Wang, L. B., & Xia, J. (2014). Face-raised octahedral Co₃O₄ nanocrystals and their catalytic activity in the selective oxidation of alcohols. *The Journal of Physical Chemistry C*, 118(9), 4767-4773.
12. Hossain, M. D., Dey, S., Mayanovic, R. A., & Benamara, M. (2016). Structural and Magnetic Properties of Well-Ordered Inverted Core-Shell α -Cr₂O₃/ α -M_xCr_{2-x}O₃ (M= Co, Ni, Mn, Fe) Nanoparticles. *MRS Advances*, 1(34), 2387-2392.
13. Dey, S., Hossain, M. D., Mayanovic, R. A., Wirth, R., & Gordon, R. A. (2017). Novel highly ordered core-shell nanoparticles. *Journal of Materials Science*, 52(4), 2066-2076.
14. Athar, T., Hakeem, A., Topnani, N., & Hashmi, A. (2012). Wet Synthesis of Monodisperse Cobalt Oxide Nanoparticles [Research article]
15. Shannon, R. D. (1976). Revised effective ionic radii and systematic studies of interatomic distances in halides and chalcogenides. *Acta crystallographica section A: crystal physics, diffraction, theoretical and general crystallography*, 32(5), 751-767.

CHAPTER 3: A STUDY OF CONCENTRATION DEPENDENT OF MANGANESE INCORPORATED CORE-SHELL NANOPARTICLES

Abstract

In my previous study, I investigated geometry shape dependent manganese incorporated $\text{Co}_3\text{O}_4@\text{Mn}_x\text{Co}_{3-x}\text{O}_4$ CSNs. The results from this study showed that pseudo-spherical shaped (PS type) CSNs have a larger coercivity and exchange bias than hexagonal nanoplates shaped CSNs at 5 K. Herein I study the manganese concentration dependence of the magnetization of PS type $\text{Co}_3\text{O}_4@\text{Mn}_x\text{Co}_{3-x}\text{O}_4$ CSNs. In this study, I used the same two-step synthesis method to grow a higher manganese concentration PS type $\text{Co}_3\text{O}_4@\text{Mn}_x\text{Co}_{3-x}\text{O}_4$ CSNs. X-ray diffraction (XRD), scanning electron microscopy (SEM), transmission electron microscopy (TEM), and x-ray photoelectron spectroscopy (XPS) have been performed in order to determine the morphological and structural properties of our CSNs, whereas the magnetic properties have been characterized using a superconducting quantum interference device (SQUID) magnetometer. The XRD results indicate that the CSNs have the same spinel crystal structure throughout the core and the shell region. The average size that was obtained using the Sherrer equation for our PS type Co_3O_4 nanoparticles was 16.3 nm whereas the average size of PS type $\text{Co}_3\text{O}_4@\text{Mn}_x\text{Co}_{3-x}\text{O}_4$ CSNs was 20.5 nm. High resolution XPS results showed that the manganese concentration of the synthesized CSNs is 6.01 at%, and the oxidation state of manganese ions is Mn^{2+} . TEM results show that the size distribution of the synthesized CSNs was 20.7 nm which is in good agreement with our XRD results. Our SQUID data indicate that the core-shell nanoparticles have both AFM (due to the Co_3O_4 core) and

ferrimagnetic properties (of the shell) with a coercivity field of 416 Oe at 5 K, which is slightly larger than 5.31 Mn at% CSNs. The magnetization vs temperature data show a spin order-disorder transition at ~31 K which is close to the lower concentration batch.

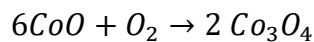
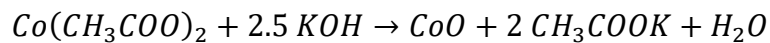
Introduction

The tunable magnetic properties of bimagnetic core-shell nanoparticles are of great interest recently. This is in good measure because bimagnetic core-shell nanoparticles have tremendous potential applications in spintronic devices, tissue engineering, drug delivery, and MRI imaging[1–5]. In addition, the exchange bias effect of the bimagnetic materials offers possibilities to establish multifunctionality (for example in magnetic random access memory). Subsequently, considerable work has been performed in this area. Munakata et al. reported that the effect of adding B can increase the anisotropy field of CoFeB thin film[6]. Liu et al. found that the higher the Ni concentration is, the lower the saturation magnetic moment per Ni atom[7]. The authors claim that this reverse relationship between doping concentration and saturation magnetic moment is because the intrinsic property of Ni-ZnO thin films, not because of any other impurity phases. Yang et al. reported that the dependence of the magnetization on electron concentration strongly confirmed the exchange mechanism for ferromagnetism in ZnO:Mn materials[8]. In previous studies in our lab, we investigated a number of different bimagnetic core-shell nanoparticles systems. One type is the inverted core-shell $\alpha\text{-Cr}_2\text{O}_3@M_x\text{Cr}_{2-x}\text{O}_{3-y}$ system (M = Co, Ni, Mn, Fe)[9], which was shown to exhibit an exchange bias effect between the antiferromagnetic Cr_2O_3 core and the ferro/ferri magnetic $M_x\text{Cr}_{2-x}\text{O}_{3-y}$ shell. Another inverted core-shell nanoparticles system investigated

in our lab is NiO@Ni_x(Mn/Co)_{1-x}O CSNs[10]. Herein, we report a novel manganese incorporated Co₃O₄@Mn_xCo_{3-x}O₄ CSN system, having a normal spinel structure. Two different manganese concentration-bearing CSNs were made using a two-step method. The primary question addressed in this study is how the magnetic properties depend on the Mn doping concentrations in the CSNs. X-ray diffraction, transmission electron microscopy, X-ray photoelectron spectroscopy, and a SQUID magnetometry were performed in order to characterize our CSNs.

Experimental

We used the same synthesis method to obtain higher concentration PS type core-shell nanoparticles [11]. Co₃O₄ nanoparticles were synthesized using a soft chemical approach¹⁴. A quantity of 0.04 M cobalt acetate was mixed with 0.1M potassium hydroxide aqueous solution to be used as a precursor. Next, we used hydrochloric acid and potassium hydroxide to adjust the pH value of the precursor solution to 9.5 and kept solution stirred for 2 hours at room temperature. Next, the solution was refluxed in a water bath at 100 °C for 4 hours. After centrifugation, the residue was rinsed thoroughly using 50% ethanol solutions, and allowed to dry at room temperature. The resulting dark grey powder was calcined at 450 °C in air for 4 hours. Subsequently, we obtained black powder. The possible chemical reactions that result in the formation of Co₃O₄ nanoparticles are shown below:



The Co_3O_4 nanoparticles were subsequently used to synthesize Co_3O_4 based $\text{Mn}_x\text{Co}_{3-x}\text{O}_4$ inverted core-shell nanoparticles using our hydrothermal Nano phase epitaxy (HNE) method³. First, 20 ml distilled water was deoxidized with dry nitrogen gas for 20 minutes at room temperature. Subsequently, 0.252 g of MnCl_2 were dissolved and sonicated in the aqueous solution for 10 minutes. Hydrochloric acid was used to control the pH value to a value of the MnCl_2 solution close to 3.5, which was subsequently mixed with 0.482 g of PS type Co_3O_4 nanoparticles. The nanoparticle-solution mixture was first sonicated 30 minutes at room temperature and then transferred to an autoclave, where it was hydrothermally treated at 200 °C for 30 hours. The resulting core-shell nanoparticles (CSN) residue was subsequently rinsed using distilled water several times, centrifuged and dried at room temperature overnight.

Characterization

X-ray diffraction (XRD) of the core-shell nanoparticles was made using a Bruker D8 Discover x-ray diffraction instrument. The x-ray diffractometer is equipped with $\text{Cu-K}\alpha$ radiation (wavelength 1.54 Å) source: The XRD data were collected covering a 2θ range from 10 to 90°. High-resolution imaging (HRTEM) and morphological characterization of the CSNs was made using an FEI Titan 80-300 transmission electron microscopy with an operating voltage of 300 KeV at the University of Arkansas. Hysteresis loop and magnetization vs temperature measurements of the CSN samples were obtained using a Quantum Design SQUID MPMS/XL magnetometer. Statistical analysis of the nanoparticles was made using imageJ in the conjunction with the TEM images. The x-ray photoemission spectroscopy measurements were made using a Versa

Probe XPS at the University of Arkansas. The X-ray source is monochromated K alpha rays from aluminum at 1486 eV; the pass energy used for surveys and high-resolution scans was 117.4 and 58.7 eV, respectively.

Results and Discussion

Fig. 3.1 (a) shows the TEM image of 0.1 M PS type $\text{Co}_3\text{O}_4@\text{Mn}_x\text{Co}_{3-x}\text{O}_4$ CSNs, showed that there was no change in shape after manganese ions incorporated in the formation of PS type $\text{Co}_3\text{O}_4@\text{Mn}_x\text{Co}_{3-x}\text{O}_4$ CSNs. Fig. 3.1 (b) shows a histogram plot of the corresponding size distribution of CSNs, from which we obtained an average size of 20.7 nm. Fig. 3.2 (a) shows a high resolution TEM image, from which we can see that the shape of isolated particle is pseudo-spherical which is consistent with our lower concentration ones. TEM-EDX results indicated the presence of manganese in the shell concentration ones. TEM-EDX results indicated the presence of manganese in the shell region of the PS type $\text{Co}_3\text{O}_4@\text{Mn}_x\text{Co}_{3-x}\text{O}_4$ CSNs (see Fig. 3.2 (b)). The same crystallographic symmetry and atomic plane continuity from core to shell, due to epitaxial growth of the shell over the core, of the CSNs is seen from our TEM results

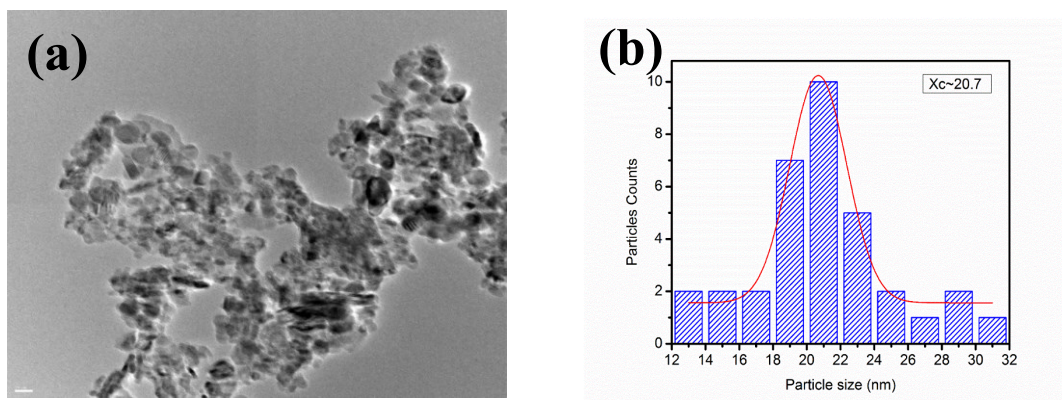


Fig. 3.1 (a) A TEM image of 0.1 M PS type $\text{Co}_3\text{O}_4@\text{Mn}_x\text{Co}_{3-x}\text{O}_4$ CSNs; (b) Corresponding size distribution of 0.1 M PS type $\text{Co}_3\text{O}_4@\text{Mn}_x\text{Co}_{3-x}\text{O}_4$ CSNs.

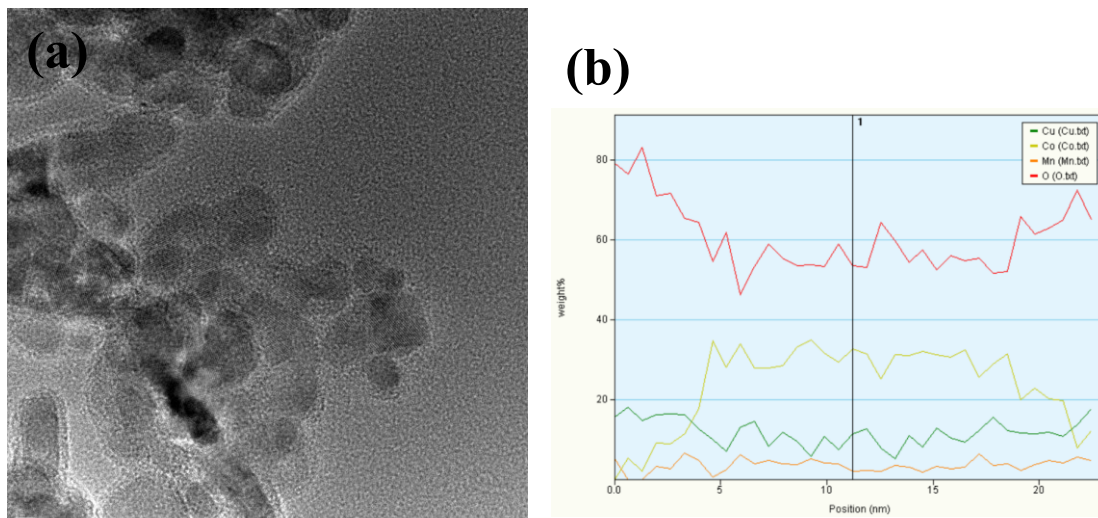


Fig. 3.2 (a) A HRTEM image of 0.1 M PS type $\text{Co}_3\text{O}_4@\text{Mn}_x\text{Co}_{3-x}\text{O}_4$ CSNs; (b) TEM-EDX of 0.1 M PS type $\text{Co}_3\text{O}_4@\text{Mn}_x\text{Co}_{3-x}\text{O}_4$ CSNs.

Fig. 3.3 shows that X-ray diffraction pattern of 0.1 M PS type $\text{Co}_3\text{O}_4@\text{Mn}_x\text{Co}_{3-x}\text{O}_4$ CSNs measured at room temperature. It is evident that 0.1 M PS type $\text{Co}_3\text{O}_4@\text{Mn}_x\text{Co}_{3-x}\text{O}_4$ CSNs maintain the same spinel structure as Co_3O_4 nanoparticles with a $F\bar{4}3m$ symmetry. There were no impurity phases in the CSNs as evidenced from the XRD data. Since the difference of the ionic radii between Mn^{2+} and Co^{2+} is small¹⁵, Mn^{2+} ions can easily replace Co^{2+} ions with minimal distortion of the spinel crystal structure of Co_3O_4 . The average size calculated using the Sherrer equation was found to be 20.5 nm, which is very close to the result obtained from size distribution analysis of the TEM images. In order to further evaluate the structural properties of CSNs, Rietveld refinement was made of the XRD data. The space group symmetry of $F\bar{4}3m$ structure was used with the starting parameters for the Co^{2+} ions at the unit cell positions $x = \frac{1}{4}$, $y = \frac{1}{4}$ and $z = \frac{1}{4}$. A second $F\bar{4}3m$ CIF file was added in order to account for the shell region in the refinement. The fitting results consistently show that the goodness-of-fit is improved significantly by use of a core-shell structure model as opposed to a single

structure model. The lattice parameters of core region and shell region were found to be 8.08(0.2) Å and 8.11(1) Å for the PS type CSNs, respectively; this slight expansion of the lattice parameter is consistent with the Shannon ionic radius of the high spin Mn^{2+} ion (0.66 Å) being slightly larger than that of high-spin Co^{2+} ion (0.58 Å) and the former partially substituting for the latter in the tetrahedral sites of the spinel structure in the shell region of the PS type CSNs.

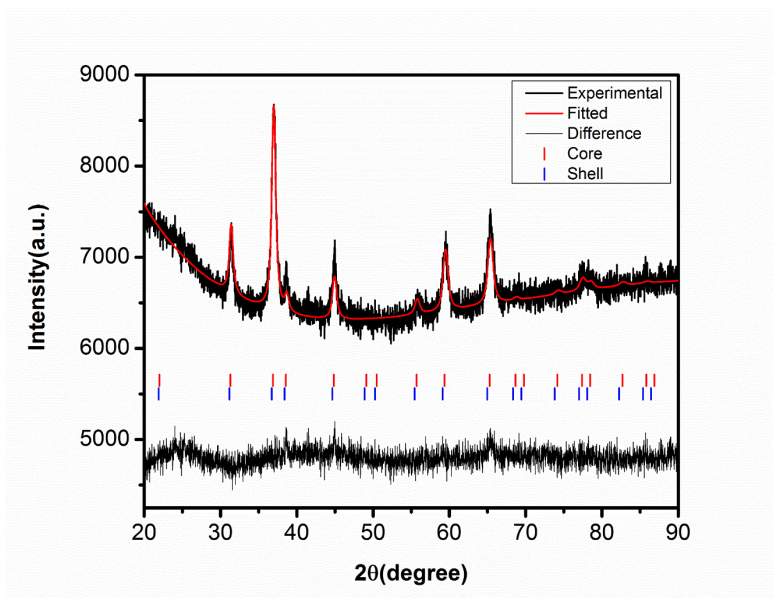


Fig. 3.3 XRD pattern of 0.1 M PS type $\text{Co}_3\text{O}_4@\text{Mn}_x\text{Co}_{3-x}\text{O}_4$ CSNs.

Fig. 3.4 (a) shows an XPS survey scan of 0.1 M PS type $\text{Co}_3\text{O}_4@\text{Mn}_x\text{Co}_{3-x}\text{O}_4$ CSNs. The presence of Mn strongly supports our TEM-EDX and XRD results, which indicate that Mn was successfully incorporated in the spinel structure of Co_3O_4 . Analysis of the XPS survey spectrum shows that the 0.1 M PS type CSNs possess 6.01 Mn at%. High resolution XPS data show that oxidation states of cobalt ions are Co^{2+} and Co^{3+} whereas the oxidation of manganese is Mn^{2+} only (Fig. 3.4 (b) and Fig. 3.4 (c)), which indicate that manganese was incorporated into tetrahedral site of the spinel structure of Co_3O_4 and successfully replaced Co^{2+} ions. I also observed a shake-up peak from HRXPS

peak of Mn 2p_{3/2}. Detailed analysis showed that there are two different types of Co binding: one is bonded with oxygen (Co-O) and the other one is bonded with hydroxyl ion (Co-OH) (see Fig. 3.4 (b)). Quantitative analysis of our high resolution XPS Mn 2p_{3/2}, Co 2p 3/2 and O 1s peaks (see reference 3 for further details on the procedures) yields a concentration of 6.01 Mn at% in the shell region of the 0.1 M PS type Mn_xCo_{3-x}O₄ CSNs (see Table 3.1).

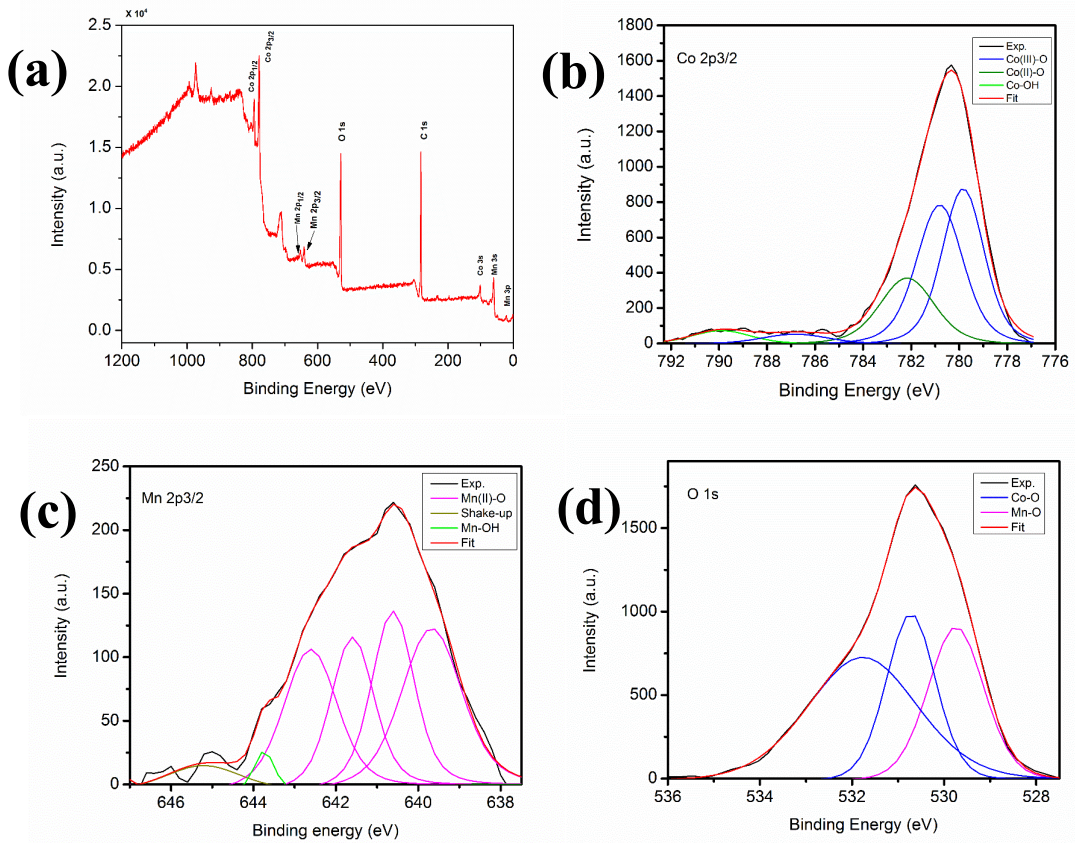


Fig. 3.4 (a) Survey scan of 0.1 M PS type Co₃O₄@Mn_xCo_{3-x}O₄ CSNs. High resolution XPS peak of (b) Co 2p_{3/2}, (c) Mn 2p_{3/2}, (d) O 1s.

Table 3.1 Chemical composition obtained from XPS data

Samples	Mn At %	Co At %	O At %
0.07 M PS type CSNs	5.31	30.51	64.18
0.1 M PS type CSNs	6.01	30.62	63.36

Fig. 3.5 (a) shows the field cooled (FC) and zero field cooled (ZFC) hysteresis loops measured from the PS type $\text{Co}_3\text{O}_4@\text{Mn}_x\text{Co}_{3-x}\text{O}_4$ CSNs at 5 K, whereas the insets show enlarged views of the M vs H data measured at 5 K. The coercivity shown in the FC hysteresis loop for the 0.1 M PS type $\text{Co}_3\text{O}_4@\text{Mn}_x\text{Co}_{3-x}\text{O}_4$ CSNs is ~410 Oe whereas the coercivity for the 0.07 M PS type $\text{Co}_3\text{O}_4@\text{Mn}_x\text{Co}_{3-x}\text{O}_4$ CSNs is ~300 Oe. The FC magnetization saturation values for the PS type CSNs at 5 K is approximately 0.39 emu/g. The FC vs zero field cooled (ZFC) hysteresis loops do not show significant shifts either in the negative or positive H axis directions. The exchange bias was calculated based on the formula $H_e = |H_{ZFC+} - H_{FC+} - H_{FC-} + H_{ZFC-}|/2$ where the +/- indicate positive/negative H values when M=0. The exchange bias for the PS type CSNs was ~35 Oe whereas for the 0.07 M PS type CSNs it was ~33 Oe, as measured at 5 K. Our magnetometry data shows that our Co_3O_4 nanoparticles and the core regions are antiferromagnetic, whereas the incorporated Mn-substituted Co_3O_4 ($\text{Mn}_x\text{Co}_{3-x}\text{O}_4$) spinel phase of the shell region is ferrimagnetic. Thus, our CSNs have the inverted core-shell magnetic configuration. Fig. 3.5 (b) show FC and ZFC magnetization vs temperature data measured from our PS type CSNs in the range from 5 to 300 K. These data show a spin order-disorder transition at ~31 K and a superparamagnetic blocking temperature of ~90 K for both types of CSNs. Fig. 3.7 shows field cooled hysteresis loops measured at different temperatures. It is apparent from the figure that the magnetization of our CSNs

decreases with increasing temperature. The temperature dependence of the coercivity and exchange bias values are shown in Fig. 3.6 (a) and (b). Both of the coercivity vs. temperature and exchange bias vs. temperature data show an exponential decay curve: The coercivity and exchange bias at 5 K are 410 Oe and 35 Oe, respectively.

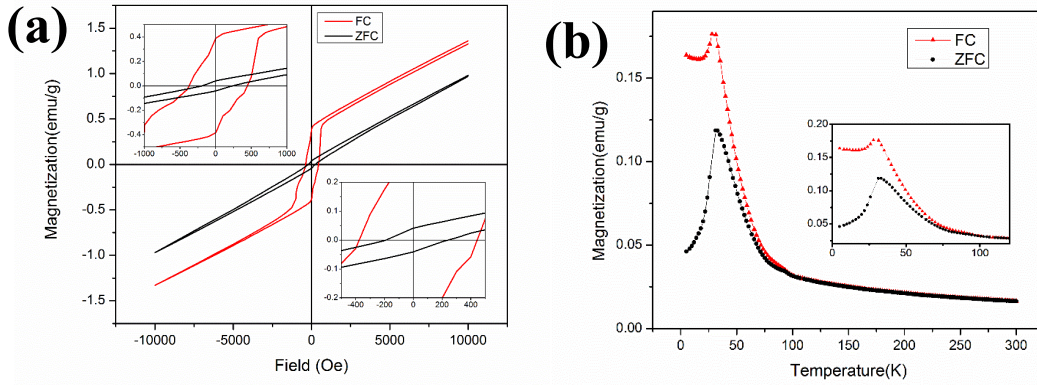


Fig. 3.5 (a) FC and ZFC hysteresis loop measured from 0.1 M PS type $\text{Co}_3\text{O}_4@\text{Mn}_x\text{Co}_{3-x}\text{O}_4$ CSNs at 5 K; the insets show enlarged views of M vs. H data. (b) FC and ZFC magnetization vs. temperature data of 0.1 M PS type $\text{Co}_3\text{O}_4@\text{Mn}_x\text{Co}_{3-x}\text{O}_4$ CSNs; the inset shows an enlarged view of M vs. T data. The FC and ZFC data were measured at an applied field of 300 Oe.

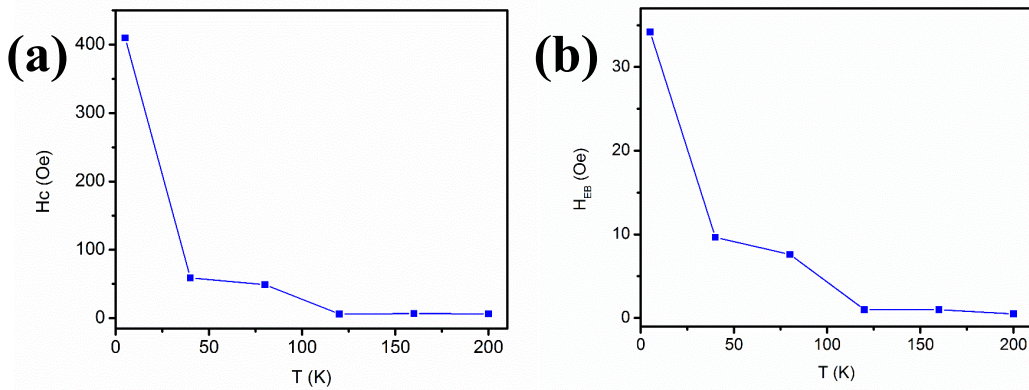


Fig. 3.6 (a) Coercivity vs. temperature data, (b) exchange bias vs. temperature data of 0.1 M PS type $\text{Co}_3\text{O}_4@\text{Mn}_x\text{Co}_{3-x}\text{O}_4$ CSNs.

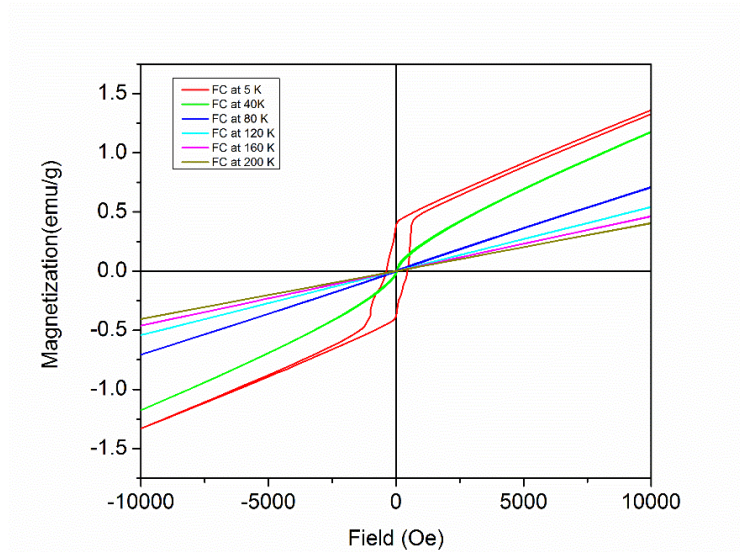


Fig. 3.7 Field cooled hysteresis loops at different temperature from 5 K to 200 K of 0.1 M PS type $\text{Co}_3\text{O}_4@\text{Mn}_x\text{Co}_{3-x}\text{O}_4$ CSNs

Conclusions

I have successfully synthesized 0.1 M PS type $\text{Co}_3\text{O}_4@\text{Mn}_x\text{Co}_{3-x}\text{O}_4$ CSNs by using a two-step synthesis process, the first involving a soft chemical approach and the second our HNE method to develop the core-shell nanostructure. The characterization results confirmed that manganese ions were incorporated into the shell region of the PS type CSNs. The TEM results explicitly show that 0.1 M PS type CSNs have a core-shell structure and epitaxial registry of shell layers on core atomic layers. The XRD results confirm that both the core region and shell region of 0.1 M PS type CSNs have the spinel structure with $F\bar{4}3m$ symmetry. The SQUID magnetometry data confirm that the 0.1 M PS type CSNs have the inverted magnetic configuration with an AFM core and FiM shell.

References

1. Lopez-Ortega, A., Estrader, M., Salazar-Alvarez, G., Roca, A. G., & Nogues, J. (2015). Applications of exchange coupled bi-magnetic hard/soft and soft/hard magnetic core/shell nanoparticles. *Physics Reports*, 553, 1-32.
2. Liu, J. P., Fullerton, E., Gutfleisch, O., & Sellmyer, D. J. (Eds.). (2009). *Nanoscale magnetic materials and applications*. Springer Science+ Business Media, LLC.
3. Hossain, M. D., Mayanovic, R. A., Sakidja, R., Benamara, M., & Wirth, R. (2018). Magnetic properties of core-shell nanoparticles possessing a novel Fe (II)-chromia phase: an experimental and theoretical approach. *Nanoscale*.
4. Vestal, C. R., & Zhang, Z. J. (2003). Synthesis and magnetic characterization of Mn and Co spinel ferrite-silica nanoparticles with tunable magnetic core. *Nano Letters*, 3(12), 1739-1743.
5. Nogués, J., Sort, J., Langlais, V., Skumryev, V., Surinach, S., Munoz, J. S., & Baró, M. D. (2005). Exchange bias in nanostructures. *Physics Reports*, 422(3), 65-117.
6. Munakata, M., Aouki, S. I., & Yagi, M. (2005). B-concentration dependence on anisotropy field of CoFeB thin film for gigahertz frequency use. *IEEE transactions on magnetics*, 41(10), 3262-3264.
7. Liu, X., Lin, F., Sun, L., Cheng, W., Ma, X., & Shi, W. (2006). Doping concentration dependence of room-temperature ferromagnetism for Ni-doped ZnO thin films prepared by pulsed-laser deposition. *Applied Physics Letters*, 88(6), 062508.
8. Yang, Z., Liu, J. L., Biasini, M., & Beyermann, W. P. (2008). Electron concentration dependent magnetization and magnetic anisotropy in ZnO: Mn thin films. *Applied Physics Letters*, 92(4), 042111.
9. Hossain, M. D. (2016). Experimental And Theoretical Analyses Of The Structural, Electronic And Magnetic Properties Of Novel Inverted Core-Shell a-CR2O3@a-Mxcr2-Xo3-Y (M= Co, Ni, Mn, Fe) Nanoparticles.
10. Hasan, S. (2017). A Study of Manganese and Cobalt Incorporated Nickel Oxide Based Core-Shell Magnetic Nanoparticles.
11. Athar, T., Hakeem, A., Topnani, N., & Hashmi, A. (2012). Wet Synthesis of Monodisperse Cobalt Oxide Nanoparticles [Research article]

CHAPTER 4: SUMMARY

In the first part of my thesis work, I studied two different morphologies of $\text{Co}_3\text{O}_4@\text{Mn}_x\text{Co}_{3-x}\text{O}_4$ CSNs by using a two-step synthesis process, the first involving a soft chemical approach and the second our HNE method to develop the core-shell nanostructure. The size of pseudo-spherical shaped (PS type) CSNs was determined by XRD and TEM to be 19.8 nm, with an average shell thickness of ~ 1.3 nm. Whereas for the hexagonal nanoplate (NP) shaped CSNs, the average diameter obtained from TEM results was ~ 188.7 nm with a thickness of ~ 9 nm. The combined XRD and TEM-EDX results confirmed that manganese ions were incorporated into the shell region of both the PS type and NP type CSNs. Our TEM results explicitly show that both the PS and NP type morphologies have an explicit core-shell structure and epitaxial registry of shell layers on core atomic layers. The XRD results confirm that both the core region and shell region of PS type and NP type CSNs have the spinel structure with $F\bar{4}3m$ symmetry. The XPS results show that the oxidation state of manganese is Mn^{2+} only with no additional oxidation states found for the element. High resolution XPS results gives Mn concentrations of 5.31 at% and 2.98 at% in PS type and NP type CSNs, respectively. SQUID magnetometry data confirm that our CSNs have the inverted magnetic configuration with an AFM core and FiM shell, whereas the PS type CSNs have a higher coercivity than NP type CSNs at 5 K.

The second part of my thesis work involved the study of the concentration dependence of magnetization of 0.1 M PS type CSNs. The PS type CSNs were synthesized using the same method as used in the first part of my study. XRD and TEM

results yielded a consistent size of the CSNs of ~20.5 nm. TEM results confirmed that the shape of the PS type nanoparticles doesn't change after the hydrothermal treatment. Furthermore, these results show that a distinct core-shell structure and epitaxial registry of shell layers on the core atomic layers. The combined results of XRD, XPS survey scan, and TEM-EDX confirmed that manganese was successfully incorporated into the shell region of the 0.1 M PS type CSNs. A Mn 6.01 at% was obtained from the analysis of the XPS spectra. High resolution XPS results confirmed that Mn is in the 2+ oxidation state in 0.1 M PS type CSNs. The coercivity at 5 K of 0.1 M PS type CSNs was ~410 Oe, which is slightly larger than that of the 0.07 M PS type CSNs.

References

1. Berkowitz, A. E., & Takano, K. (1999). Exchange anisotropy — a review. *Journal of Magnetism and Magnetic Materials*, 200(1), 552–570.
2. Fan, S., Wang, W., Ke, H., Rao, J.-C., & Zhou, Y. (2016). Bimagnetic urchin-like Co₃O₄/CoFe₂O₄ nanocomposites: synthesis and magnetic properties. *RSC Advances*, 6(99), 97055–97062.
3. Fan, Y., Smith, K. J., Lüpke, G., Hanbicki, A. T., Goswami, R., Li, C. H., ... Jonker, B. T. (2013). Exchange bias of the interface spin system at the Fe/MgO interface. *Nature Nanotechnology*, 8(6), 438–444.
4. Fontaíña-Troitiño, N., Liébana-Viñas, S., Rodríguez-González, B., Li, Z.-A., Spasova, M., Farle, M., & Salgueiriño, V. (2014). Room-Temperature Ferromagnetism in Antiferromagnetic Cobalt Oxide Nanooctahedra. *Nano Letters*, 14(2), 640–647.
5. Gawande, M. B., Goswami, A., Asefa, T., Guo, H., Biradar, A. V., Peng, D.-L., Varma, R. S. (2015). Core-shell nanoparticles: synthesis and applications in catalysis and electrocatalysis. *Chemical Society Reviews*, 44(21), 7540–7590.
6. González, J. A., Andrés, J. P., López Antón, R., De Toro, J. A., Normile, P. S., Muñiz, P., ... Nogués, J. (2017). Maximizing Exchange Bias in Co/CoO Core/Shell Nanoparticles by Lattice Matching between the Shell and the Embedding Matrix. *Chemistry of Materials*, 29(12), 5200–5206.

7. Hossain, M. D., Mayanovic, R. A., Sakidja, R., Benamara, M., & Wirth, R. (2018). Magnetic properties of core-shell nanoparticles possessing a novel Fe(II)-chromia phase: an experimental and theoretical approach. *Nanoscale*, *10*(4), 2138–2147.
8. Ignatiev, P. A., Negulyaev, N. N., Bazhanov, D. I., & Stepanyuk, V. S. (2010). Doping of cobalt oxide with transition metal impurities: *Ab initio* study. *Physical Review B*, *81*(23).
9. Li, W. Y., Xu, L. N., & Chen, J. (2005). Co₃O₄ Nanomaterials in Lithium-Ion Batteries and Gas Sensors. *Advanced Functional Materials*, *15*(5), 851–857.
10. Liu, J. P., Fullerton, E., Gutfleisch, O., & Sellmyer, D. J. (Eds.). (2009). *Nanoscale Magnetic Materials and Applications*. Springer US. Retrieved from [//www.springer.com/us/book/9780387855981](http://www.springer.com/us/book/9780387855981)
11. López-Ortega, A., Estrader, M., Salazar-Alvarez, G., Roca, A. G., & Nogués, J. (2015). Applications of exchange coupled bi-magnetic hard/soft and soft/hard magnetic core/shell nanoparticles. *Physics Reports*, *553*, 1–32.
12. Lottini, E., López-Ortega, A., Bertoni, G., Turner, S., Meledina, M., Van Tendeloo, G., Sangregorio, C. (2016). Strongly Exchange Coupled Core|Shell Nanoparticles with High Magnetic Anisotropy: A Strategy toward Rare-Earth-Free Permanent Magnets. *Chemistry of Materials*, *28*(12), 4214–4222.
13. Lou, X. W., Deng, D., Lee, J. Y., & Archer, L. A. (2008). Thermal formation of mesoporous single-crystal Co₃O₄ nano-needles and their lithium storage properties. *Journal of Materials Chemistry*, *18*(37), 4397–4401.
14. Meiklejohn, W. H., & Bean, C. P. (1956). New Magnetic Anisotropy. *Physical Review*, *102*(5), 1413–1414.
15. Naveen, A. N., & Selladurai, S. (2015). Tailoring structural, optical and magnetic properties of spinel type cobalt oxide (Co₃O₄) by manganese doping. *Physica B: Condensed Matter*, *457*, 251–262.
16. Nogués, J., & Schuller, I. K. (1999). Exchange bias. *Journal of Magnetism and Magnetic Materials*, *192*(2), 203–232.
17. Park, H.-Y., Schadt, M. J., Wang, Lim, I.-I. S., Njoki, P. N., Kim, S. H. Zhong, C.-J. (2007). Fabrication of Magnetic Core@Shell Fe Oxide@Au Nanoparticles for Interfacial Bioactivity and Bio-separation. *Langmuir*, *23*(17), 9050–9056.
18. Roth, W. L. (1964). Magnetic properties of normal spinels with only a-a interactions. *Journal de Physique*, *25*(5), 507–515.

19. Wang, X., Tian, W., Zhai, T., Zhi, C., Bando, Y., & Golberg, D. (2012). Cobalt (II,III) oxide hollow structures: fabrication, properties and applications. *Journal of Materials Chemistry*, 22(44), 23310–23326.
20. Xie, X., Li, Y., Liu, Z.-Q., Haruta, M., & Shen, W. (2009). Low-temperature oxidation of CO catalysed by Co(3)O(4) nanorods. *Nature*, 458(7239), 746–749.
21. Xu, Z., Hou, Y., & Sun, S. (2007). Magnetic Core/Shell Fe₃O₄/Au and Fe₃O₄/Au/Ag Nanoparticles with Tunable Plasmonic Properties. *Journal of the American Chemical Society*, 129(28), 8698–8699.